Experimental Investigation of Electrostatic Effect on Particle Motions in Gas-Solid Fluidized Beds

Kezeng Dong, Qing Zhang, Zhengliang Huang, Zuwei Liao, Jingdai Wang, Yongrong Yang, and Fang Wang
State Key Laboratory of Chemical Engineering, Dept. of Chemical and Biological Engineering, Zhejiang University, Hangzhou, 310027 China

DOI 10.1002/aic.14933
Published online July 14, 2015 in Wiley Online Library (wileyonlinelibrary.com)

The excess accumulation of charges in the fluidized bed has a severe impact on hydrodynamics. Due to lack of effective experimental methods, electrostatic effects on hydrodynamics have mostly been studied using numerical simulation. By injecting a trace of liquid antistatic agents into a fluidized bed, charges were controlled and electrostatic influences on particle motions were investigated. The average particle–wall impact angles are acquired by developing multiscale wavelet decomposition of acoustic emission signals. The impact angles are significantly influenced by both charge levels and gas velocities. If the electric force is reduced and/or fluid drag is increased, friction dominates the particle–wall interactions. Under a larger gas velocity where fluid drag dominates, charges elimination causes no significant variation in particle impact angles, but particle velocities increase as well as at lower gas velocities. In addition, existence of electrostatic charges influences the ranges of bubble growing zone and jet impacting zone. © 2015 American Institute of Chemical Engineers *AIChE J*, 61: 3628–3638, 2015
Keywords: fluidized bed, electrostatic, particle motion, impact angle, acoustic emission technique

Introduction

Particle motions and circulations in freely bubbling fluidized beds are mainly driven by arising gas bubbles. Particles move upward through bubble wake regions and particle velocities are significantly influenced by bubble sizes and velocities. On one hand, particle velocity will impact important hydrodynamic parameters like particles residence time, gas-solid contacting efficiency, and axial solid diffusion.[1] On the other hand, particle motions cause impact and friction between particles and particle–wall, which result in electrostatic charges generation and accumulation. Triboelectric charging between particles is mainly determined by materials, particle sizes, relative velocity, and environmental conditions.[2–5] Except for these essentials, tribocharging between particles and wall is still influenced by particle impact angles.[6,7] He et al.[7] studied the influence of collision angle on current transferred from particles to probe and found the polarity of transferred current changed from positive to negative as collision angle increased. On the contrary, the influence of charges of moving particles on impact angle has never been investigated.

The excess accumulation of electrostatic charges in the fluidized bed has a severe impact on hydrodynamics and even causes particle agglomeration and wall sheeting.[8–13] When particles are charged, particle motions are not only impacted by fluid drag and gravity, but also influenced by electric force, including electrostatic attraction and repulsion between particles and particle–wall.[14–20] Restricted particle motions and distribution due to electric force are the main cause of particle agglomeration and wall sheeting. However, due to lack of effective experimental methods, electrostatic effects on particle motions in the fluidized bed have mostly been studied through numerical simulation by limited researchers. Rokkam et al.[21,22] developed a multifluid computational fluid dynamics (CFD) simulation coupled with a simple electrostatic model and studied electrostatic effects on particle segregation, fines elutriation, and wall sheeting in industrial polyolefin fluidized bed reactors. Hassani et al.[19] developed a discrete element method coupled with CFD model to investigate the influence of electrostatics on hydrodynamics and indicated that the existence of monocharged particles resulted in the decrease of gas bubble sizes and solid diffusion coefficient. Lim[18] numerically studied the electrostatic effects on mixing behaviors of binary particles and indicated that particle velocity reduced and particles tended to adhere to wall, when electric force between particle–wall dominated. This author also recommended experimental investigations on electrostatic influences to verify the simulation results. Most numerical simulations coupled with electrostatic model involve several assumptions which significantly deviate from truth. For instance, there is no charge generation and dissipation during fluidization. However, electrostatic charges in the fluidized beds stay in dynamic equilibrium rather than unchanged. In addition, most simulation results have not been verified by experiments. Therefore, it is of vital importance to develop experimental investigation of electrostatic influences on fluidized particle motions.

In fluidized beds, acoustic emission (AE) signals are mostly generated from friction and impact between particle–particle

Correspondence concerning this article should be addressed to J. Wang at wangjd@zju.edu.cn.

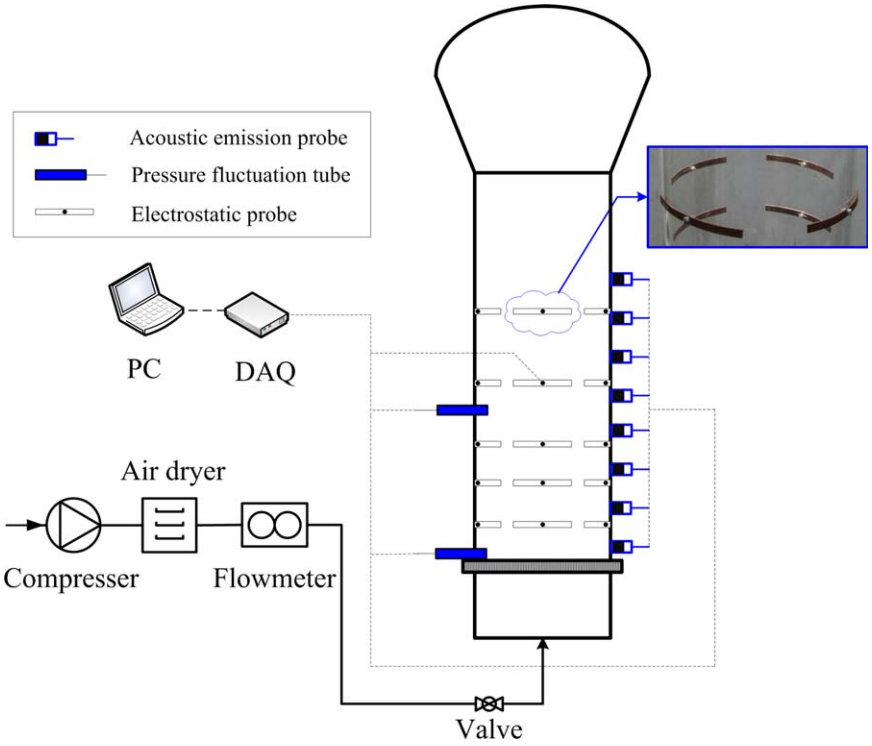

Figure 1. Schematic diagram of experimental apparatus.

[Color figure can be viewed in the online issue, which is available at wileyonlinelibrary.com.]

and particle–wall.[23–28] As a nonintrusive, real-time monitoring method, AE technique has been widely used in various chemical engineering processes, especially in particulate processes.[29–32] Cody et al.[33] developed particles granular temperature calculation model based on AE signals on column wall and studied the influence of particle sizes and superficial gas velocity on particles granular temperature. The authors[34] further indicated that particle velocities, solid phase pressure, and diffusion coefficients can be acquired from AE signals. Tsujimoto et al.[26] used the high frequency AE sensors to study the hydrodynamics in the fluidized bed and found that the amplitudes of AE signals were related to dimensionless gas velocity and initial bed height. Wang et al.[35,36] also studied particle granular temperature using AE technique and developed particle flow pattern recognition method based on AE signals. He et al.[37] developed a powder mass flow rate detection model in pneumatic conveying system based on the relative magnitude of collision and friction energy ratio from multiscale wavelet analysis of AE signals from tube wall using high-frequency AE sensors. Therefore, the nonintrusive AE technique can be applied to study particle motions and flow patterns in the fluidized bed.

In our previous study,[38] trace amounts of liquid antistatic agents (LAAs) were applied to control the charge levels of fluidized particles and electrostatic effects on bubble behaviors were experimentally investigated. The results showed charge accumulation resulted in significant decrease of bubble sizes and bed level fluctuations. Since particle motions are mainly driven by rising gas bubbles, variations of bubble sizes should strongly influence particle motions simultaneously. However, electrostatic effects on particle motions have been hardly investigated so far, experimentally. Therefore, this work provides a first insight into electrostatic effects on fluidized particle motions experimentally by injecting different amounts of LAA contents and using AE technique. Electrostatic influences on particle impact angles and particle flow patterns were specially focused on and a comparison of electric force and fluid force under various conditions was also made.

Experimental Methods and Materials

Figure 1 shows the schematic diagram of the experimental apparatus, which consists of fluidization system and measurement system. The solid line represents gas flow while the dashed line stands for signal flow. The fluidized bed is made of a transparent Plexiglas column with an inner diameter of 150 mm and a height of 1000 mm. The expanded section at the column top has a height of 300 mm and a width of 250 mm. At the bottom of bed column, an iron perforated distributor with open area ratio of 2.6% is installed, along with a gas mixing chamber. Compressed air predried to a relative humidity of 5–10% and within the temperature range of 10–15°C is used as the fluidizing gas.

The measurement system includes online AE system, pressure fluctuations, and electrostatic current detection system. The online AE system consists of an AE sensor, a preamplifier, a main amplifier, data acquisition card (NI, USB-6351), and a personal computer.[30,36] The AE sensor used in this work is a piezoelectric accelerometer, which has a resonance frequency of 140 kHz (AE 144S, Fuji Ceramics Corp.). The sensors are mounted on the outside of the column wall, collecting signals generated from particle–wall impact and friction at various axial heights (50–500 mm above the distributor). According to the Shannon sampling theory,[39] the sampling frequency was chosen as 500 kHz and the sampling time is 5 s. The pressure fluctuations were measured at heights of 20 and 180 mm above the distributor using two pressure tubes, which were made of steel with a length of 80 mm and an internal diameter of 4 mm. Each tube was flush mounted with the

Table 1. LAA Injection Amount

Mass ratio, ppm	12.5	37.5	62.5
Volume, mL	0.03	0.09	0.15

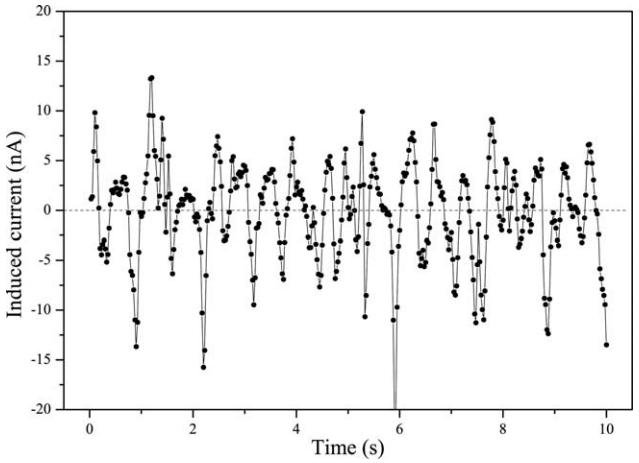

Figure 2. Variations of induced currents with time.

(H = 90 mm, $U - U_{mf}$ = 0.15 m/s).

inner wall of the column with a fine mesh covering the tip to prevent fine particles from entering. The probe was connected to one of two channels of a differential pressure transducer (CTG121P, China), which produced an output voltage proportional to the pressure difference between the two channels. The other channel was exposed to the atmosphere, therefore, the absolute pressure was acquired. The measuring range of the pressure transducer is ±2 kPa, and its relative accuracy is ±0.25% of full scale. The sampling frequency of pressure fluctuation is 400 Hz and sampling time is 5 min. The electrostatic current detection system includes multiple-induced electrostatic probes and an electrometer (NanoCoulomb Meter 284, Monroe Electronics). The copper made arc-shaped electrostatic probes, with a width of 6 mm and thickness of 2 mm, were attached on the outer surface of the fluidized bed at a 60° angle, as shown in Figure 1. The arc-shaped electrodes were set at five different levels (90, 180, 230, 300, and 380 mm above the distributor), with four electrodes at the same level.

Table 2. Average Induced Currents

$U - U_{mf}$ (m/s)	LAA (ppm)	IC(+) (nA)	Std (nA)	IC(−) (nA)	Std (nA)
0.15	0	31.3	11.6	−30.5	10.9
0.15	12.5	21.2	7.9	−21.7	7.7
0.15	37.5	16.1	4.5	−16.9	4.7
0.15	62.5	3.2	0.4	−3.2	0.6
0.35	0	123.5	21.4	−120.4	25.4
0.35	12.5	111.1	11.7	−108.8	21.6
0.35	37.5	30.8	4.9	−33.7	4.5
0.35	62.5	8. 4	0.8	−8.3	1.1

When charged particles come across the probes, induced currents are generated, the magnitudes of which can be used to characterize the charge level of fluidized particles.[40]

The polypropylene (PP) particles (Sinopec, China), with particle density of 0.9 g/cm^3 and mean diameter of 1.85 mm (Geldart D type), were used as fluidized particles. PP particles used in this work are the same as those reported in our previous work,[38] from which the sieve size distribution was shown. The minimum fluidization velocity was determined experimentally from the pressure drop vs. superficial gas velocity curve and found to be 0.55 m/s. Experiments were carried out under excess superficial velocities of 0.15 and 0.35 m/s, respectively.

Atmer^{TM} 163 is a commonly used LAA in polyolefin industry to control the charge level of fluidized particles. Different amounts of LAA were injected in this work, as shown in Table 1.

Results and Discussions

Control of electrostatic charge levels in fluidized bed

Various amounts of LAA were injected to maintain different charge levels of fluidized particles, enabling the influence of electrostatics on particle motions to be studied. Figure 2 shows the variations of induced currents with time after fluidization for 30 min. The electrodes may sense both the charges of fluidized particles and the charges of the column wall. When particles are fully charged after a certain fluidization time, the charges of particles and the column wall should tend to reach equilibrium state. Therefore, the currents induced from the column wall should be constant. However, according to the variations of induced currents in Figure 2, the induced currents still significantly fluctuate with time. The fluctuation of induced currents were attributed to the motion of charged

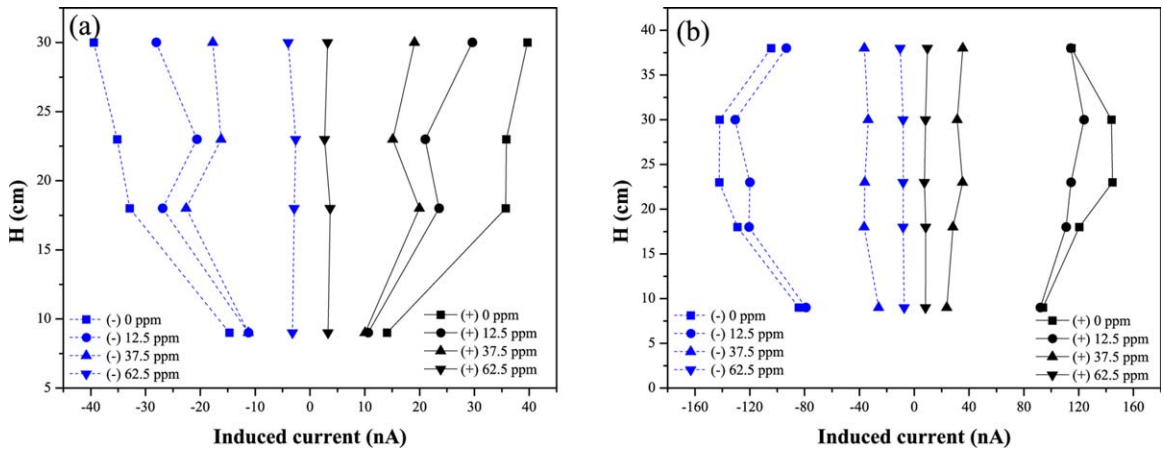

Figure 3. Variation of induced currents at multiple positions.

(a) $U - U_{mf}$ =0.15 m/s. (b) $U - U_{mf}$ =0.35 m/s. [Color figure can be viewed in the online issue, which is available at wileyonlinelibrary.com.]

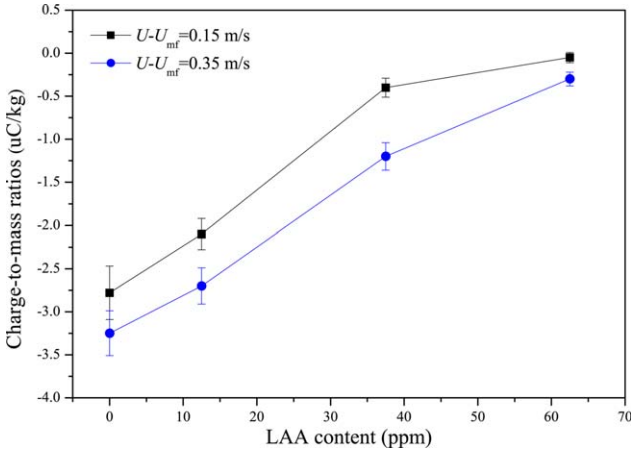

Figure 4. Variations of charge-to-mass ratios under various LAA contents at two excess gas velocities.

($H = 80$ mm). [Color figure can be viewed in the online issue, which is available at wileyonlinelibrary.com.]

particles through sense zone of electrodes, thus both positive and negative currents are generated. The amplitude of induced currents is mainly influenced by the charges of particles and particle velocities.[40] Therefore, under a certain fluidization condition, the mean amplitude of induced currents can be used to characterize the charge of particles.

Figure 3 shows the variations of mean induced current at multiple axial positions. At a lower excess gas velocity (0.15 m/s), no obvious current was found on the electrode set at 380 mm, therefore, variations of induced currents at four positions were displayed in Figure 3a.

In a freely bubbling fluidized bed without LAA, the average induced current at excess superficial gas velocities of 0.15 and 0.35 m/s was determined to be 31.3 and 123.5 nA, respectively. The induced currents significantly decreased after injection of LAA and particle charges were nearly completely eliminated after an injection of 62.5 ppm LAA. The mean induced currents at various axial positions are shown in Table 2. As shown in Table 2, the average induced currents significantly decrease with increasing LAA content.

Figure 4 further shows the variations of charge-to-mass ratios under various LAA contents and two excess gas velocities. Particles at the bottom part ($H = 80$ mm) were negatively charged. Since the LAA increases the charge dissipation rate, the charge-to-mass ratios (absolute value) decreases with the increase of LAA contents. Particles were more negatively charged under a larger excess gas velocity (0.35 m/s) and the influences of LAA on charge-to-mass ratios were similar. Therefore, according to the results of induced currents and charge-to-mass ratios, the charge levels in fluidized bed can be controlled via injection of trace LAA.

Figure 5 shows the variations of standard deviations (STD) of pressure fluctuations at different charge levels under two superficial gas velocities. As shown in Figure 5a, the STD increases significantly with increasing injection amounts of LAA at an excess superficial gas velocity of 0.15 m/s, which indicates a smaller charge level in the fluidized bed, resulted in the formation of larger bubbles. When the excess gas velocity was increased to 0.35 m/s, the STD only increased slightly with increasing LAA contents. Suppose the magnitude of STD can be used as a characteristic length of bubble size,[41,42] significant differences of the electrostatic effect on bubble sizes under different gas velocities can be observed. From Figure 5, the largest STD increases due to electrostatic elimination at an excess gas velocity of 0.15 and 0.35 m/s is 62 and 12%, respectively. However, from Table 2, the largest decrease in induced currents is 28 and 115 nA. The results indicate that a larger decrease in charge level does not necessarily translate to a large increase in bubble size. The influence of excess superficial gas velocity should be accounted when considering the electrostatic effect on bubble sizes. This is due to the difference of the dominant forces on the particles under different gas velocities, which will be further discussed in the following section.

Electrostatic effect on fluidized particle motions

The charge levels of fluidized particles can be controlled by injecting various amounts of LAA, therefore, influence of electrostatics on particle motions can be further studied. AE signals were used in this work to characterize particle motions. Figure 6 shows the comparison of AE time domain signals and power spectral density (PSD) analysis at different charge levels of fluidized particles. The frequency information of AE signals was mainly located between 15 and 150 kHz and two dominant frequency peaks at 20–60 and 60–120 kHz, respectively, can be easily found from Figure 6. When the charge

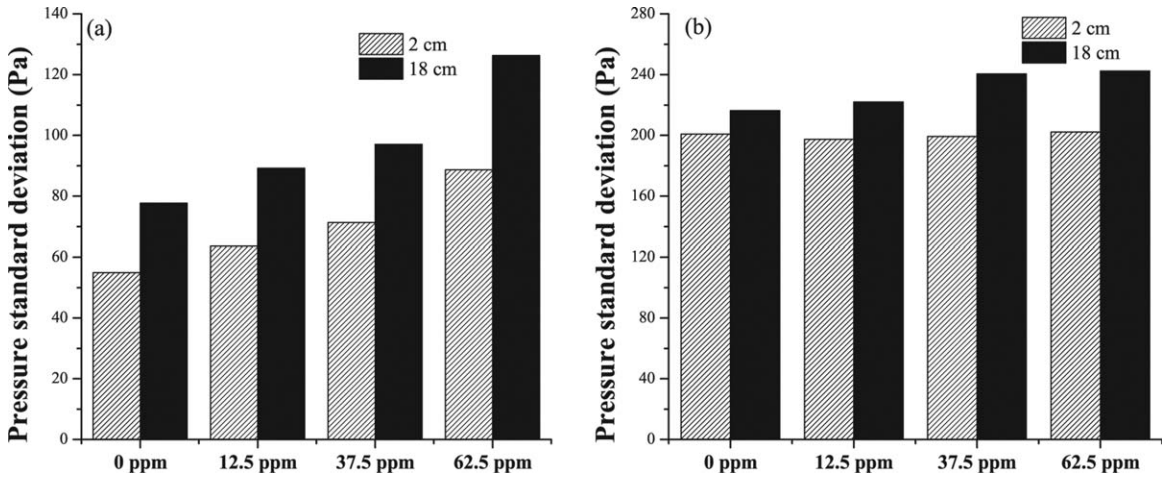

Figure 5. Variations of standard deviations of pressure fluctuations with various LAA contents.

(a) $U - U_{mf} = 0.15$ m/s. (b) $U - U_{mf} = 0.35$ m/s.

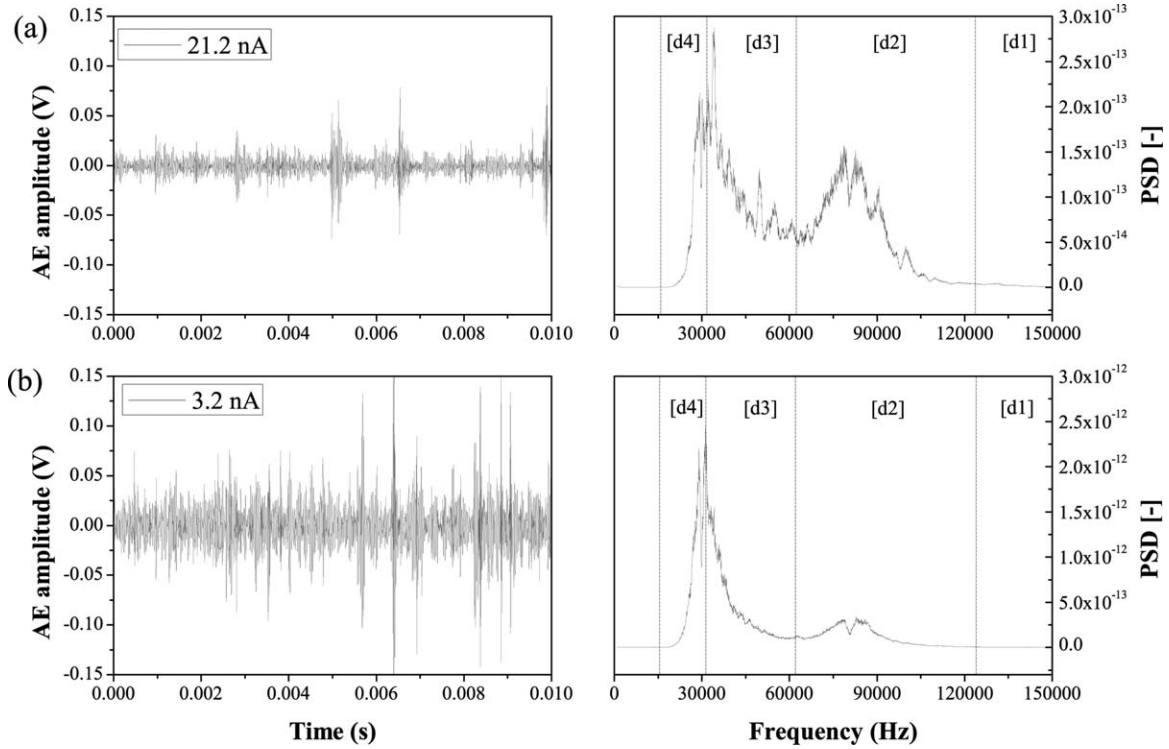

Figure 6. AE time domain signals and PSD analysis in different charge levels.

(a) $U - U_{mf} = 0.15$ m/s, $H = 7.5$ cm, IC $= 21.2$ nA; (b) $U - U_{mf} = 0.15$ m/s, $H = 7.5$ cm, IC $= 3.2$ nA.

level decreased from 21.2 to 3.2 nA, the magnitude of AE signal significantly increased, an indicator of a stronger particle motion. The higher frequency peak in the PSD was obviously decreased due to charge decrease, while the magnitude of PSD significantly increased.

In fluidized beds, the AE signals were mostly generated from friction and impact between particle–particle and particle–wall. Since the AE signals attenuate rapidly in air,[26] the signals acquired in this work from the column wall are mainly due to friction and impact between fluidized particles and wall. He et al.[37] developed wavelet analysis on AE signals acquired from the pneumatic conveying pipeline and found the AE energy consisted of friction energy and impact energy. To be specific, the friction energy lay in the frequency range of 0–60 kHz and while the impact energy was mainly in the range of 60–120 kHz, which was in good accordance to our results in Figure 6. Therefore, their analysis was adopted in this work.

The AE energy of particle–wall impact and friction can be separately expressed as[36,37]

$$E_c = 2\eta t m C_s S_p v_{p,n}^3 \tag{1}$$

$$E_f = 2\mu\eta t m C_s S_p v_{p,t} v_{p,n}^2 \tag{2}$$

where C_s is the particles concentration near the wall, S_p is the valid receiving area of AE sensor, $v_{p,n}$ and $v_{p,t}$ stands for the normal and tangential impact velocity between particles and wall, η is the transformation efficiency from collision pressure to acoustic pressure, μ is the friction efficient, m is the mass of single particle, and t represents the detection time. When the materials are fixed, the total AE energy is only related to particle velocity, particle concentration, and impact angle α

$$E_t = E_c + E_f = 2\eta t m C_s S_p v_{p,n}^3 \left(1 + \frac{\mu}{\tan\alpha}\right) \tag{3}$$

In order to further acquire the impact energy and friction energy between particle–wall, 5 scales wavelet decomposition of AE signals was developed. The frequency of each scale wavelet is listed in Table 3, which is also shown in Figure 6.

Figures 7 and 8 showed the time domain and PSD analysis of 5 scales wavelet decomposition signals. As shown in Figure 7, the main time domain information is located in the scales of 1–4. In addition, the main frequency information is almost included in first 4 scale signals and located between 15.6 and 125 kHz, to be specific. Moreover, the frequency information of first two scales lay in 62.5–125 kHz and that of 3rd and 4th lay in 15.6–62.5 kHz, which was exactly the same frequency range of two dominant frequency peaks in Figure 6. In other words, the first two scales wavelet decomposition signals can be used to represent the particle–wall impact while the 3rd and 4th scale signals stood for particle–wall friction.

Therefore, the impact energy and friction energy based on AE signals can be defined

$$D_c = \frac{E_c}{E_t} = \frac{1}{\frac{\mu}{\tan\alpha} + 1} = d_1 + d_2 \tag{4}$$

Table 3. Frequency Ranges of the 5 Scales Wavelet Decomposition Signals

Scale	d1	d2	d3	d4	d5	a5
f (kHz)	125–250	62.5–125	31.3–62.5	15.6–31.3	7.81–15.6	0–7.81

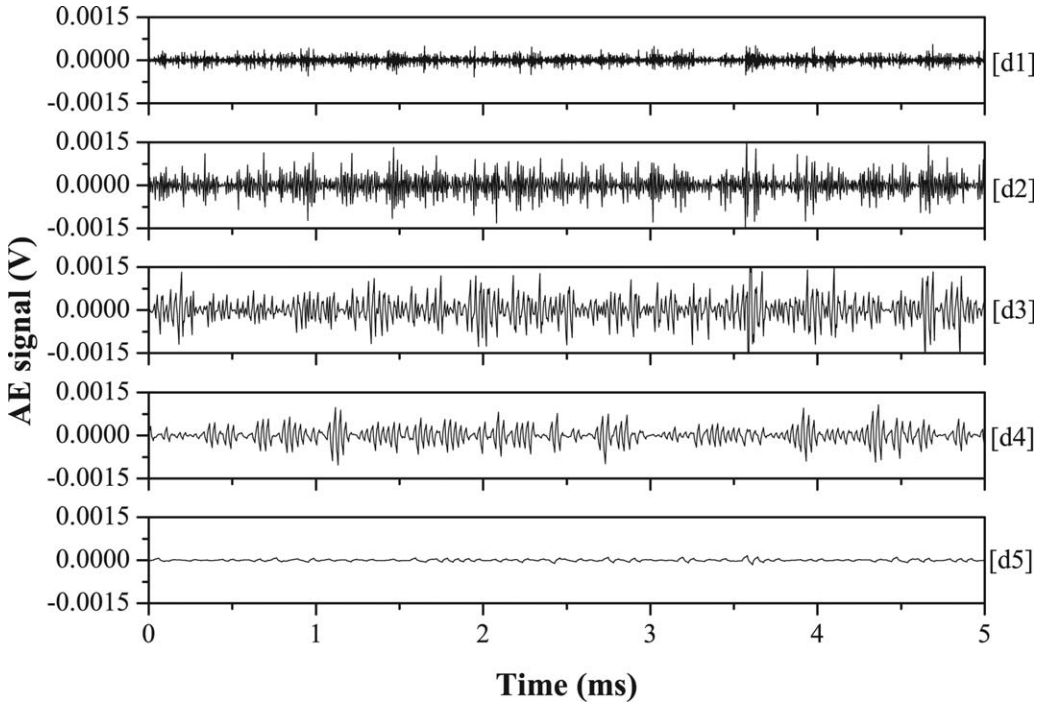

Figure 7. Reconstruction of each scale wavelet decomposition time domain signals.

($U - U_{mf} = 0.15$ m/s, 12.5 ppm, $H = 17.5$ cm).

$$D_f = \frac{E_f}{E_t} = \frac{\frac{\mu}{\tan\alpha}}{\frac{\mu}{\tan\alpha}+1} = d_3 + d_4 \quad (5)$$

where D_c and D_f represent particle–wall impact energy ratio and friction energy ratio, respectively, and d_1–d_4 represent the wavelet scale energy ratio. The impact angle can be further derived from Eq. 4

$$\alpha = \frac{\mu D_c}{1 - D_c} \quad (6)$$

Therefore, the impact angle α between particles and wall can be calculated from friction coefficient and impact energy ratio.

Figure 9 showed the electrostatic effect on axial distribution of impact energy ratio D_c and friction energy ratio D_f under

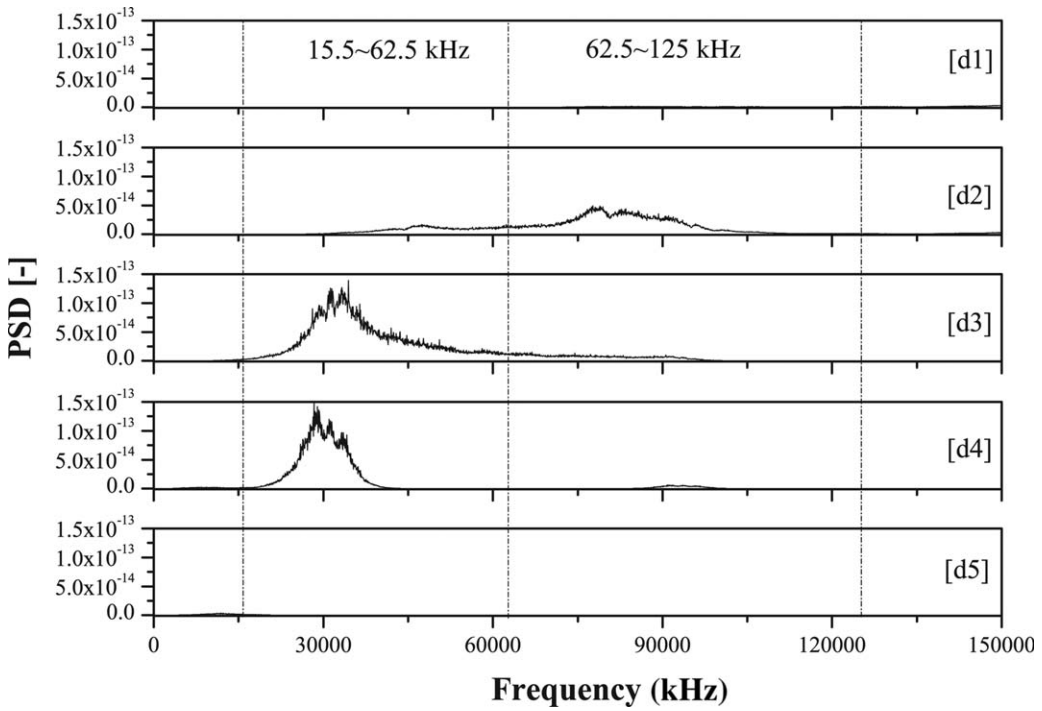

Figure 8. PSD analysis of each scale wavelet decomposition signals.

($U - U_{mf} = 0.15$ m/s, 12.5 ppm, $H = 17.5$ cm).

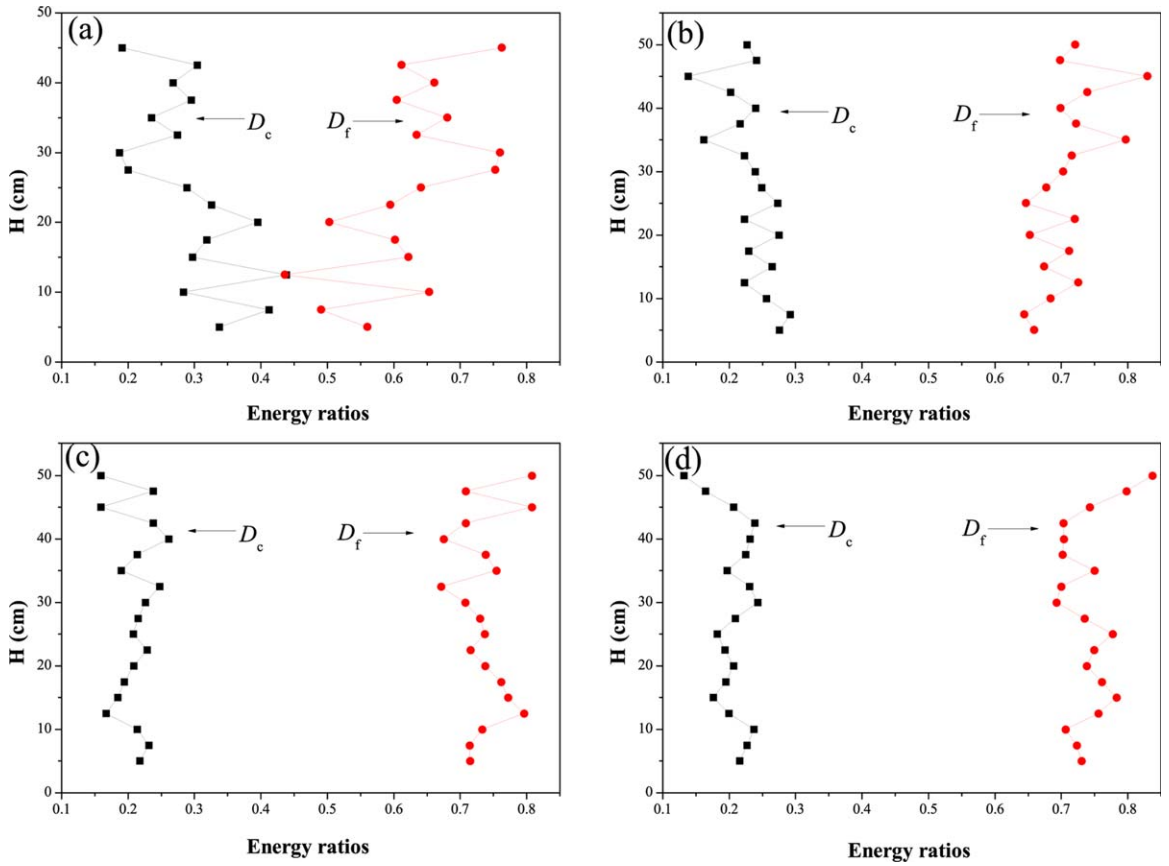

Figure 9. Axial distribution of impact energy ratio *Dc* and friction energy ratio D_f in fluidized bed.

(a) $U - U_{mf} = 0.15$ m/s, 0 ppm. (b) $U - U_{mf} = 0.35$ m/s, 0 ppm. (c) $U - U_{mf} = 0.15$ m/s, 62.5 ppm. (d) $U - U_{mf} = 0.35$ m/s, 62.5 ppm. [Color figure can be viewed in the online issue, which is available at wileyonlinelibrary.com.]

two excess superficial gas velocities. D_f was significantly larger than D_c in every case studied, which indicated that friction dominated the interaction between particles and wall. The friction and impact energy ratio were influenced by both gas velocity and charge levels of particles. As shown in Figure 9a, when particles were fully charged at a low gas velocity, the impact energy ratio at the column bottom was obviously larger than that at the top. On the contrary, the friction energy ratio at the bottom was relatively small. However, the impact energy ratio at the bottom reduced significantly after increasing the excess superficial gas velocity (Figure 9b) or charge neutralization (Figure 9c), thus, keeping both D_c and D_f almost constant in multiple axial positions. On the one hand, increasing the gas velocity raised the drag force on particles, which mainly acted in the axial direction like gas flow. Thus, the friction energy ratio increased and impact energy ratio decreased after raising gas velocity. On the other hand, reduction of charge levels led to a decrease of electrostatic force, resulting in the drag becoming the dominant force. Therefore, reducing electrostatic charges translated into an increase of D_f and decrease of D_c.

Moreover, electrostatic charges elimination resulted in a significant increase of friction energy ratio under an excess gas velocity of 0.15 m/s while a larger excess gas velocity weakened the electrostatic effect. This can be attributed to the dominance of the drag force at large gas velocities and meanwhile the electrostatic effects on particle motions were less significant. Lim's[18] simulation results also indicated that electrostatic force influence on particle velocity and mixing behaviors decreased with increasing gas velocity.

According to Eq. 6, the impact angle can be calculated from friction coefficient (assumed as 0.3[43]) and impact energy ratio. Figure 10 displayed the axial distribution of impact angles under various LAA contents. When particles were charged, the mean impact angle at the bottom of fluidized bed was larger than that at the top, where particle–wall friction dominated. Most fluidized particles were ejected from the bubble wakes at bed level and then moved downward along the column wall.[25] Therefore, those particles near the wall at the top only had a tiny impact angle (close to 5°) and friction dominated the particle–wall interaction. However, for particles near the wall at the bottom, their velocities were not only influenced by other downward moving particles, but also by gas jet and bubble coalescence. Therefore, the normal velocity of these particles was larger than that at the top, which resulted in a larger impact angle. When charges were fully or partly eliminated at a lower gas velocity, electrostatic forces between particles and wall reduced. Thus, particle motions were mainly controlled by drag force. Therefore, normal velocities and impact angles decreased. However, under an excess gas velocity of 0.35 m/s, electrostatic influence on impact angles weakened, mainly due to the dominance of the drag force at a higher gas velocity.

As shown in Figure 10, electrostatic charges mainly influenced particles at the bottom. Figure 11 further showed the results of electrostatic influence on impact angles of particles at the heights below 300 mm. Under an excess gas velocity of 0.15 m/s, the mean impact angle decreased from 8° to 5° due to electrostatic charges elimination. Increasing the gas velocity

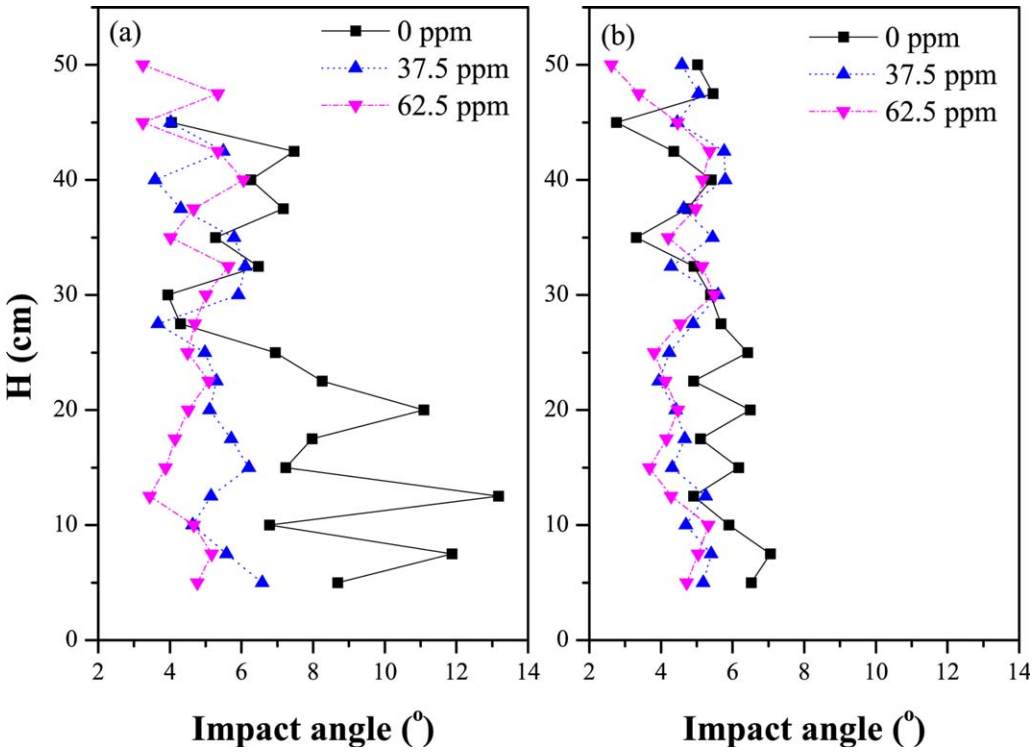

Figure 10. Axial distribution of impact angles under various LAA contents.

(a) $U - U_{mf} = 0.15$m/s. (b) $U - U_{mf} = 0.35$ m/s. [Color figure can be viewed in the online issue, which is available at wileyonlinelibrary.com.]

weakened the electrostatic effect. In addition, the impact angles at two different superficial gas velocities were both close to 5° after charge elimination. When charges were eliminated, particle motions were mainly influenced by fluid drag, under which particle–wall friction dominated. In addition, the fluid drag in the emulsion is mainly influenced by the rise velocity of emulsion gas, which is determined by the minimum gas velocity. Therefore, the mean impact angles near the wall did not change much at two superficial gas velocities when particles were uncharged.

Comparison of electrostatic force and drag force

As aforementioned, electrostatic charges had significant effects on particle motions under a relatively small gas velocity and electrostatic influence strongly weakened at a larger gas velocity. When particles were charged, particle motions were simultaneously influenced by gravity, fluid drag, and electrostatic force. The relative magnitude of drag and electrostatic force determined the electrostatic influence on particle motions. A comparison of electrostatic force and drag force was developed based on theoretical estimation.

Hendrickson[13] concluded three estimation methods of maximum charge density of fluidized particles and indicated the calculation method developed by Revel et al.[44] gave a more reasonable result and can be expressed as

$$\left|\frac{Q}{M}\right|_{\max} = \frac{\varepsilon_0 E_d \pi D H}{M} \tag{7}$$

where E_d is breakdown electric field strength ($E_d = 3 \times 10^6$ V/m for air), D and H stands for column diameter and height, M is the total weight of particles. The electrostatic force on particles with a maximum charge density is[13]

$$|F|_{e,\max} = E \cdot |q|_{\max} = 166.82 \frac{d_p^3}{(1-\varepsilon)D} \tag{8}$$

Conversely, the fluid drag can be describe as

$$F_d = \frac{1}{2} C_D \rho_f \left(v_f - v_p\right)^2 \frac{\pi d_p^2}{4} \tag{9}$$

where C_D is the drag coefficient and related to particles' Re_p[45]

$$C_D = \begin{cases} \dfrac{24}{Re_p}\left(1 + 0.15\left(Re_p\right)^{0.687}\right); & Re_p < 1000 \\ 0.44; & Re_p \geq 1000 \end{cases} \tag{10}$$

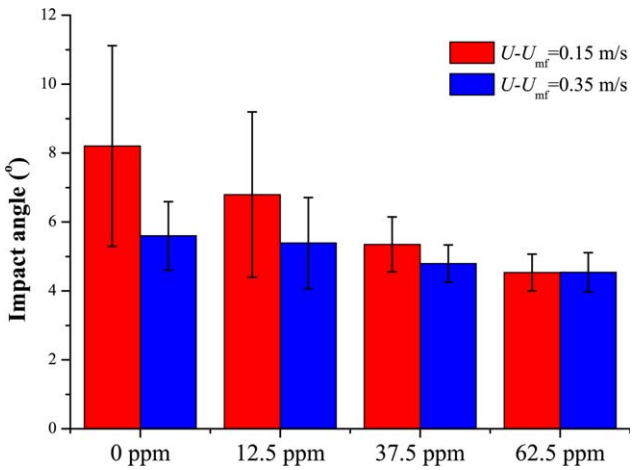

Figure 11. Electrostatic influence on mean particle–wall impact angles.

[Color figure can be viewed in the online issue, which is available at wileyonlinelibrary.com.]

where Re_p is defined as

$$Re_p = \frac{\varepsilon \rho_f (v_f - v_p) d_p}{\mu_f} \quad (11)$$

The drag coefficient defined in Eq. 10 was applied to single particle motion in the fluid. Since particle motions were influenced by other adjacent particles in the fluidized bed, Wen and Yu[46] developed the following correction to show the effect due to the presence of other particles

$$C_{Da} = C_D \varepsilon^{-4.7} \quad (12)$$

The maximum charge density calculated from Eq. 7 was 6.25 μC/kg. However, the maximum charge to mass ratio acquired from experiments was only 3.25 μC/kg, less than 50% of theoretical estimation. Hendrickson[13] indicated that the deviation of theoretical and measured particle electrostatic charges can be attributed to the wide variation in experimental conditions. It is still uncertain whether the saturation charge depends only on particles or also depends on fluidized bed parameters. The estimation method (Eq. 7) obviously overpredicted the saturation charge in this work. The existence of gas humidity was also accounted for the deviation. The influence of relative humidity of fluidizing gas on particle charges was investigated and shown in Figure 12, which indicated a significant increase of charges (absolute value) with the decrease of relative humidity, even under a relative small relative humidity. All the previous experiments were carried out with 5–10% humidity. In addition, contact de-electrification[47] of electrostatically charged polymers should also be accounted.

Figure 13 showed a comparison of electrostatic force and drag force under various gas velocities for PP particles with a diameter of 1.85 mm, gravity was also listed as a reference of magnitude. As shown in Figure 13, the maximum electrostatic force and fluid drag was of the similar order of magnitude and the drag increased significantly with increasing superficial gas velocity. When particles were charged with 50% $(q/m)_{max}$, which was more reasonable comparing to experimental value, electrostatic force was of the same order of magnitude as fluid drag under a low gas velocity ($U_0 = 0.7$ m/s, $U_0 - U_{mf} = 0.15$ m/s). On the one hand, electrostatic force existed in both axial and radial directions, and the radial electric force was even larger.[48] On the other hand, the fluid drag mainly acted

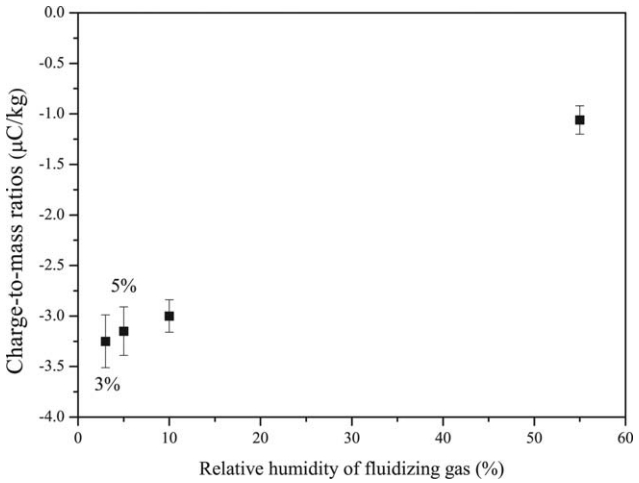

Figure 12. Influence of relative humidity of fluidizing gas on particle charges.

($H = 80$ mm, $U - U_{mf} = 0.35$ m/s).

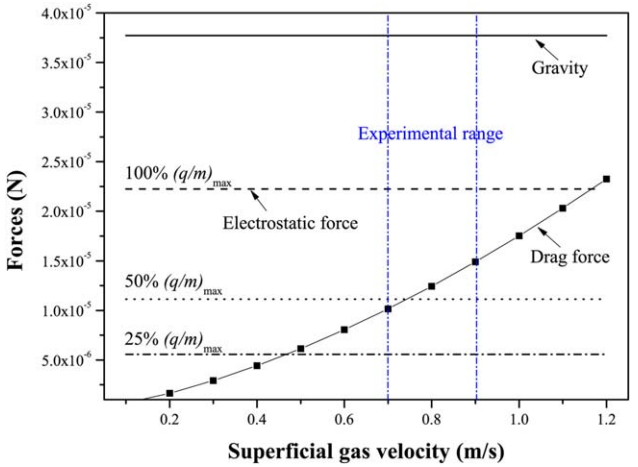

Figure 13. A comparison of electrostatic force and drag under various gas velocities.

(polypropylene, $d_p = 1.85$ mm, $U_{mf} = 0.55$ m/s, $\varepsilon = 0.6$). [Color figure can be viewed in the online issue, which is available at wileyonlinelibrary.com.]

on the particles in the gas flow direction. Therefore, when the magnitude of electric force and drag was close, the existence of electric force would certainly enhance the radial motions of charged particles. Thus, the impact angel between particles and wall increased due to electrostatics existence, which was in accordance with previous results from AE detection (Figure 10). When charge levels were reduced, for example, decreasing from 50% $(q/m)_{max}$ to 25% $(q/m)_{max}$, the electric force decreased correspondingly and meanwhile, fluid drag dominated and thus impact angles reduced. When superficial gas velocity increased from 0.7 to 0.9 m/s, the fluid drag obviously increased and became dominant force since the charge density of particles never exceed 50% $(q/m)_{max}$ in all experiments studied. Therefore, electrostatic effects on particle impact angle at higher gas velocities were not as significant as those at lower gas velocities. The results from theoretical estimations were consistent with experimental findings in Figure 11.

Electrostatic effects on particle flow patterns in the fluidized bed

Electrostatic effects on particle motions have been previously investigated and it can be concluded that electrostatic charges mainly influenced the impact angles and velocities at the bottom of fluidized bed. Since particle flow patterns in the fluidized bed were determined by particle motions at multiple positions and can be characterized by axial distributions of AE energy,[35,36] the electrostatic effects on flow patterns were then studied.

Figure 14 showed the axial distributions of AE energy under various conditions. When particles were fully charged, according to Figures 13a, b, axial distributions of AE energy could be divided into three zones, (1) particles ejection zone at the top, (2) bubble growing zone at the middle part, and (3) jet impacting zone at the bottom. Gas bubbles split at the bed level and particles in wake region were ejected into the freeboard. In the freeboard, both particle concentration and particle velocity decreased with increasing height. Therefore, the AE energy in particles ejection zone decreased in the axial direction. Bubble coalescence acted in the bubble growing zone and particle velocities increased since bubble sizes enlarged in the axial direction. Thus, the AE energy raised

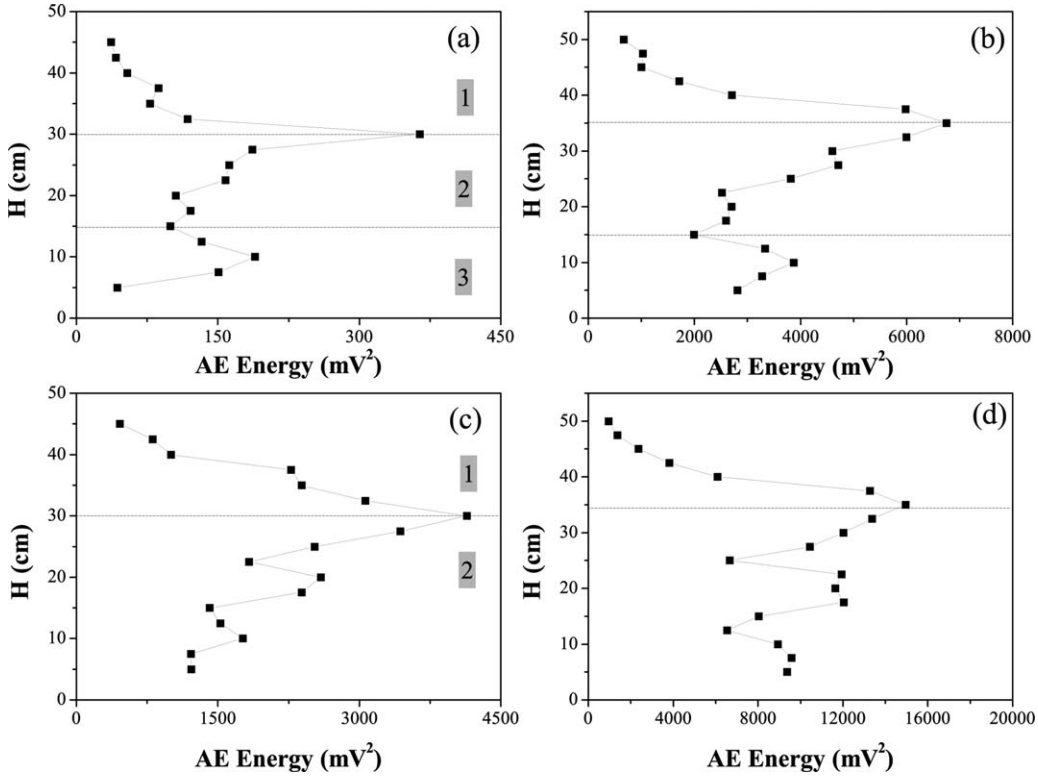

Figure 14. Axial distributions of AE energy under various conditions.

(a) $U - U_{mf} = 0.15$ m/s, 0 ppm. (b) $U - U_{mf} = 0.35$ m/s, 0 ppm. (c) $U - U_{mf} = 0.15$ m/s, 62.5 ppm. (d) $U - U_{mf} = 0.35$ m/s, 62.5 ppm.

rapidly in the bubble growing zone. In the jet impacting zone near the distributor, particle motions were mainly influenced by gas jet. Particles were first accelerated by gas jet in the flow direction and then decelerated due to gravity after leaving jet impact. Therefore, the AE energy increased at first then decreased with increasing height in jet impacting zone.

From to Figures 14a, b, increasing gas velocity did not change the particle flow pattern but only led to increase of AE energy, which was due to an increase of particle velocity. Besides, the bubble growing zone enlarged from 150 to 200 mm when the excess gas velocity was increased from 0.15 to 0.3 m/s. When electrostatic charges were eliminated, through injection of 62.5 ppm LAA, the axial AE energy generally increased for both gas velocities. Particle motions were driven by rising bubbles and bubble sizes increased due to charge elimination.[19,38] Therefore, particle velocities increased after charge elimination, which further led to increase of AE energy. In addition, the boundary between bubble growing zone and jet impacting zone became indistinct and AE energy fluctuations increased due to charge elimination. When electrostatic charges were eliminated, mean impact angles near the distributor significantly decreased and friction dominated the particle–wall interaction. Since the particle–wall frictions in axial direction were mainly influenced by rising gas bubbles, particle motions became fluctuate due to various small bubbles generated close to the distributor.

Conclusions

Electrification degree of insulated particles in fluidized bed were controlled by injecting a trace of LAA, thus electrostatic influences on particle motions can be investigated. The AE technique was applied in this work to characterize particle motions in the fluidized bed. Particles impact energy and friction energy have been acquired by developing 5 scales wavelet decomposition of AE signals. The particle–wall impact angles, calculated from the impact energy ratio, were influenced by both charge levels and gas velocities. A relative small impact angle was required at the whole bed, which indicated that the particle–wall interaction was dominated by friction for Geldart D particles studied in this work. Electrostatic charges have been found to have significant effects on particle impact angles under a relatively small gas velocity, but the electrostatic force influence strongly weakened under a larger gas velocity due to dominance of the fluid drag force in comparison to the electric force. However, the impact velocity significantly increased after charge elimination for both gas velocities studied.

The flow pattern of Geldart D particles in the fluidized bed can be divided into three zones, namely particle ejection zone, bubble rising zone, and jet impacting zone. Since particle motions were driven by rising bubbles, particle impact velocity was reduced due to electrostatic charges, as well as the bubble sizes. The boundary of bubble rising zone and jet impacting zone became indistinct after charge elimination.

Therefore, electrostatic influences on hydrodynamics should be taken into more consideration rather than those on wall sheeting and agglomeration. Electrostatics accumulation in the fluidized beds not only resulted in gas bubble reduction, but also led to decrease of particle impact velocity and bubble rising zone, which may further cause wall sheeting or particle agglomeration, especially in industrial polymerization reactors.

Acknowledgments

The authors are grateful for the financial support of this work from the National Natural Science Foundation of China (Grant No. 21236007), National Basic Research Program of China (Grant No. 2012CB720500), Specialized Research

Fund for the Doctoral Program of Higher Education (Grant No. 20130101110063) and Zhejiang Provincial Natural Science Foundation of China (Grant No. R14B060003, LQ13B060002).

Literature Cited

1. Abbasi M, Sotudeh-Gharebagh R, Mostoufi N, Zarghami R, Mahjoob MJ. Nonintrusive characterization of fluidized bed hydrodynamics using vibration signature analysis. *AIChE J*. 2010;56(3):597–603.
2. Bilici MA, Toth JR, 3rd, Sankaran RM, Lacks DJ. Particle size effects in particle-particle triboelectric charging studied with an integrated fluidized bed and electrostatic separator system. *Rev Sci Instrum*. 2014;85(10):103903.
3. Forward KM, Lacks DJ, Sankaran RM. Particle-size dependent bipolar charging of Martian regolith simulant. *Geophys Res Lett*. 2009; 36(13):L13201.
4. Forward KM, Lacks DJ, Sankaran RM. Charge segregation depends on particle size in triboelectrically charged granular materials. *Phys Rev Lett*. 2009;102(2):028001.
5. Matsusaka S, Maruyama H, Matsuyama T, Ghadiri M. Triboelectric charging of powders: a review. *Chem Eng Sci*. 2010;65(22):5781–5807.
6. Sommerfeld M, Huber N. Experimental analysis and modelling of particle-wall collisions. *Int J Multiphase Flow*. 1999;25(6–7):1457–1489.
7. He C, Bi XTT, Grace JR. Contact electrification of a novel dual-material probe with charged particulate flow. *Powder Technol*. 2014; 253:1–9.
8. Wang F, Wang J, Yang Y. Distribution of electrostatic potential in a gas-solid fluidized bed and measurement of bed level. *Ind Eng Chem Res*. 2008;47:9517–9526.
9. Dong K, Zhang Q, Huang Z, Liao Z, Wang J, Yang Y. Experimental investigation of electrostatic reduction in a gas–solid fluidized bed by an in situ corona charge eliminator. *Ind Eng Chem Res*. 2014; 53(37):14217–14224.
10. Sowinski A, Miller L, Mehrani P. Investigation of electrostatic charge distribution in gas-solid fluidized beds. *Chem Eng Sci*. 2010; 65:2771–2781.
11. Moughrabiah WO, Grace JR, Bi XT. Electrostatics in gas–solid fluidized beds for different particle properties. *Chem Eng Sci*. 2012;75: 198–208.
12. Sowinski A, Mayne A, Mehrani P. Effect of fluidizing particle size on electrostatic charge generation and reactor wall fouling in gas–solid fluidized beds. *Chem Eng Sci*. 2012;71:552–563.
13. Hendrickson G. Electrostatics and gas phase fluidized bed polymerization reactor wall sheeting. *Chem Eng Sci*. 2006;61(4):1041–1064.
14. Colver GM. An interparticle force model for ac–dc electric fields in powders. *Powder Technol*. 2000;112(1–2):126–136.
15. Kleijn van Willigen F, Demirbas B, Deen NG, Kuipers JAM, van Ommen JR. Discrete particle simulations of an electric-field enhanced fluidized bed. *Powder Technol*. 2008;183(2):196–206.
16. Lim EWC, Zhang Y, Wang C-H. Effects of an electrostatic field in pneumatic conveying of granular materials through inclined and vertical pipes. *Chem Eng Sci*. 2006;61(24):7889–7908.
17. Lim EWC, Yao J, Zhao Y. Pneumatic transport of granular materials with electrostatic effects. *AIChE J*. 2012;58(4):1040–1059.
18. Lim EWC. Mixing behaviors of granular materials in gas fluidized beds with electrostatic effects. *Ind Eng Chem Res*. 2013;52(45): 15863–15873.
19. Hassani MA, Zarghami R, Norouzi HR, Mostoufi N. Numerical investigation of effect of electrostatic forces on the hydrodynamics of gas–solid fluidized beds. *Powder Technol*. 2013;246:16–25.
20. Jiang L, Fang-Zhi X, Zheng-Hong L. A CFD modeling of the gas–solid two-phase flow in an FCC riser under the electrostatic conditions. *Asia-Pacific J Chem Eng*. 2014;9(5):645–655.
21. Rokkam RG, Fox RO, Muhle ME. Computational fluid dynamics and electrostatic modeling of polymerization fluidized-bed reactors. *Powder Technol*. 2010;203:109–124.
22. Rokkam RG, Sowinski A, Fox RO, Mehrani P, Muhle ME. Computational and experimental study of electrostatics in gas–solid polymerization fluidized beds. *Chem Eng Sci*. 2013;92(0):146–156.
23. Mostoufi N, Chaouki J. On the axial movement of solids in gas-solid fluidized beds. *Chem Eng Res Des*. 2000;78(6):911–920.
24. Azizpour H, Sotudeh-Gharebagh R, Zarghami R, Abbasi M, Mostoufi N, Mahjoob MJ. Characterization of gas-solid fluidized bed hydrodynamics by vibration signature analysis. *Int J Multiphase Flow*. 2011;37(7):788–793.
25. Stein M, Ding YL, Seville JPK, Parker DJ. Solids motion in bubbling gas fluidised beds. *Chem Eng Sci*. 2000;55(22):5291–5300.
26. Tsujimoto H, Yokoyama T, Huang CC, Sekiguchi I. Monitoring particle fluidization in a fluidized bed granulator with an acoustic emission sensor. *Powder Technol*. 2000;113(1–2):88–96.
27. Wong YS. Particle motion in relatively thin fluidised bed models. *Chem Eng Sci*. 2006;61(18):6234–6238.
28. Briongos JV, Sobrino C, Gómez-Hernández J, Santana D. Characterization of flow-induced vibrations in gas–solid fluidized beds: elements of the theory. *Chem Eng Sci*. 2013;93:181–196.
29. Boyd JWR, Varley J. The uses of passive measurement of acoustic emissions from chemical engineering processes. *Chem Eng Sci*. 2001;56(5):1749–1767.
30. Cao Y, Wang J, He Y, Liu W, Yang Y. Agglomeration detection based on attractor comparison in horizontal stirred bed reactors by acoustic emission sensors. *AIChE J*. 2009;55(12):3099–3108.
31. Abbasi M, Mostoufi N, Sotudeh-Gharebagh R, Zarghami R. A novel approach for simultaneous hydrodynamic characterization of gas-liquid and gas-solid systems. *Chem Eng Sci*. 2013;100:74–82.
32. Afsahi F-A, Sotudeh-Gharebagh R, Mostoufi N. Clusters identification and characterization in a gas–solid fluidized bed by the wavelet analysis. *Can J Chem Eng*. 2009;87(3):375–385.
33. Cody GD, Goldfarb DJ, Storch GV, Jr, Norris AN. Particle granular temperature in gas fluidized beds. *Powder Technol*. 1996;87(3):211–232.
34. Cody GD, Bellows RJ, Goldfarb DJ, Wolf HA, Storch Jr GV. A novel non-intrusive probe of particle motion and gas generation in the feed injection zone of the feed riser of a fluidized bed catalytic cracking unit. *Powder Technol*. 2000;110(1–2):128–142.
35. Wang J, Ren C, Yang Y, Hou L. Characterization of particle fluidization pattern in a gas solid fluidized bed based on acoustic emission (AE) measurement. *Ind Eng Chem Res*. 2009;48(18):8508–8514.
36. Jingdai W, Congjing R, Yongrong Y. Characterization of flow regime transition and particle motion using acoustic emission measurement in a gas-solid fluidized bed. *AIChE J*. 2010;56(5):1173–1183.
37. He L, Zhou Y, Huang Z, Wang J, Lungu M, Yang Y. Acoustic analysis of particle–wall interaction and detection of particle mass flow rate in vertical pneumatic conveying. *Ind Eng Chem Res*. 2014; 53(23):9938–9948.
38. Dong K, Zhang Q, Huang Z, Liao Z, Wang J, Yang Y. Experimental investigation of electrostatic effect on bubble behaviors in gas-solid fluidized bed. *AIChE J*. 2015;61(4):1160–1171.
39. Turner JD, Pretlove A. *Acoustics for engineers*. Basingstoke: Macmillan, 1991.
40. Zhang W, Cheng Y, Wang C, Yang W, Wang C-H. Investigation on hydrodynamics of triple-bed combined circulating fluidized bed using electrostatic sensor and electrical capacitance tomography. *Ind Eng Chem Res*. 2013;52(32):11198–11207.
41. Bi H, Chen A. Pressure fluctuations in gas-solids fluidized beds. *China Particuol*. 2003;1(4):139–144.
42. Bi HT. A critical review of the complex pressure fluctuation phenomenon in gas-solids fluidized beds. *Chem Eng Sci*. 2007;62:3473–3493.
43. Chuan Lim EW, Hee Tan RB, Xiao Z. Mixing behaviors of wet granular materials in gas fluidized bed systems. *AIChE J*. 2013; 59(11):4058–4067.
44. Revel J, Gatumel C, Dodds JA, Taillet J. Generation of static electricity during fluidisation of polyethylene and its elimination by air ionisation. *Powder Technol*. 2003;135–136:192–200.
45. Rowe P, Henwood G. Drag forces in a hydraulic model of a fluidised bed. *Trans Inst Chem Eng*. 1960;39:175–180.
46. Wen C, Yu Y. Mechanics of fluidization. *Chem Eng Prog Symp Ser*. 1966;62(62):100.
47. Soh S, Kwok SW, Liu H, Whitesides GM. Contact de-electrification of electrostatically charged polymers. *J Am Chem Soc*. 2012; 134(49):20151–20159.
48. Jalalinejad F, Bi XT, Grace JR. Effect of electrostatic charges on single bubble in gas–solid fluidized beds. *Int J Multiphase Flow*. 2012;44:15–28.

Manuscript received Mar. 4, 2015, and revision received June 15, 2015.